

# The coating of FeB, FeTi, FeW powders on AISI 430 stainless steel by PTA

T. TEKER<sup>a,\*</sup>, S. KARATAŞ<sup>b</sup>, S. O. YILMAZ<sup>b</sup>

<sup>a</sup>University of Adiyaman, Faculty of Engineering, Department of Materials Engineering, 02040, Adiyaman, Turkey

<sup>b</sup>University of Firat, Faculty of Engineering, Department of Metallurgical and Materials, 23117, Elazığ, Turkey

In-situ synthesized TiB<sub>2</sub>, Fe<sub>2</sub>B reinforced Fe based coating was fabricated on an AISI 430 steel substrate by plasma transfer arc process (PTA) with FeB, FeTi, FeW powders. The effects of the process parameters on the coating were investigated experimentally. The surfaces were subsequently characterized by SEM, EDS and XRD to differentiate the effect of coating parameters on the microstructure. Primary ferrite ( $\alpha$ ) phase dendrites and complex TiB<sub>2</sub>, Fe<sub>2</sub>B borides around the dendrites were detected on the subsurface microstructure. The experimental results show that the distribution of boron and titanium is not homogeneous on either the coated surface or interface microstructures. The difference in hardness of the microstructures is specifically attributed to the type of borides.

(Received August 9, 2012; accepted April 11, 2013)

*Keywords:* Microanalysis, Intermetallic, Plasma transferred arc, Hardening

## 1. Introduction

In recent years, in situ synthesis of boride and carbide reinforced metal matrix composites surfaces, which were produced by using plasma transferred arc (PTA), gas tungsten arc welding (GTAW) and laser beam techniques, have received much interest in world-wide [1]. They put forward elimination of interfacial incompatibility of matrices with reinforcements by creating more thermodynamically stable reinforcements based on their nucleation and growth from the parent matrix phase [1]. The PTA surfacing process is characterized by extremely high temperatures, excellent arc stability, low thermal distortion of the part, and high coating speeds [1]. PTA has a potential to be used for surface modification [2-3]. Surface roughness and thickness of the heat affected zone is serious problems in the GTAW method [4], and laser beam methods is expensive and difficult comparing complex components using the PTA method [4,5]. Recently, the PTA process have been used widely to achieve a surface composites coatings, where the alloying powders feed externally to melting bath and a thin surface layer is simultaneously melted and then solidified [5]. The PTA process has an advantage of using two independent arcs (i.e. non-transferred arc as pilot and transferred arc as main arc). This advantage may play a role in allowing proper microstructural development and was used in the present study to investigate its effect on the resulting coating properties. The PTA system works by passing argon gas through an inert annulus between the cathode and anode and is ionised, forming a constricted plasma arc column, which provides a current path for a transferred arc. The PTA process was widely used for the surface treatment of materials and developed as a modification of the plasma arc welding method [2].

Fe based metal matrix composites have extensive applications in tools, dies and wear as well as high temperature oxidation resistance components. Ferrous matrix composites have a wide range of applications because of their high mechanical strength. Serious techniques are being used to produce high performance composites to improve the interfacial compatibility and to avoid serious interfacial reactions. The in-situ technique is being used as a new technique for the production of ceramic particle reinforced metal matrix composites (MMCs) [1-4]. The in-situ processing technique depends on a basic principle: thermodynamically stable phases having fine sizes are formed by an exothermal reaction between elements and compounds within the metal matrix. This process has some advantages; the reinforced surface generated in-situ tends to remain free of contamination, such as gas absorption, oxidation and other detrimental surface reactions. The mentioned advantages produce an improved reinforcement matrix interface bond. In addition, the composites produced by the in-situ process exhibit improved mechanical strength, hardness, as well as enhanced wear resistance [5,6]. The production of Fe based composites or coated surfaces through the in-situ process with titanium diboride (TiB<sub>2</sub>) has been examined in literature [5-8]. Titanium diboride (TiB<sub>2</sub>) is the most inert, stiff, and hardest of all the borides [7], and has high mechanical strength and high resistance to wear and high tensile strength at high temperatures. In contrast to most ceramics, it is electrically and thermally conductive [7,8]. These properties suggest that TiB<sub>2</sub> is a potential reinforcing material for the wear applications where high thermal conductivity is important. These properties lead to its use in shields elements. The major advantage is that they eliminate the interfacial incompatibility of matrices with reinforcements by creating more thermodynamically

stable reinforcements based on their nucleation and growth from the parent matrix phase. Recently, the in-situ synthesis of TiB<sub>2</sub> reinforced metal matrix surfaces composites materials was reported. TiB<sub>2</sub> particles were successfully synthesized in microstructures [9]. It is desirable that the surface layer of components is reinforced by TiB<sub>2</sub> particles to offer high wear resistance to them whilst they retain the high toughness and strength [10-15]. Fe, Ni and Co are the most suitable metals as they have appropriate melting points and very good wetting properties on TiB<sub>2</sub> [16]. Most of the TiB<sub>2</sub>-(Fe,Ni) materials which have been developed so far have metallic phases with a Fe:Ni weight-ratio near to 70:30 as they exhibit not only excellent wetting properties on TiB<sub>2</sub> but also very low thermal expansion coefficients [17]. Research on these materials has been mainly focused on the prevention of the formation of secondary borides (M<sub>3</sub>B, M<sub>3</sub>B<sub>4</sub>, where M:Fe, Ni, Ti) which cause resentment of these materials [18,19]. It is important to avoid the formation of undesirable secondary borides.

The objective of this study is to produce a coated surface having TiB<sub>2</sub> hard phases with a minimum production cost. In addition to establish relationships between the chemical compositions and microstructure and decreasing the undesirable secondary borides in the microstructure. The PTA is suggested to process TiB<sub>2</sub>

reinforced Fe-based surface coating by evenly depositing B, Ti and W based alloy powders.

## 2. Experimental procedures

A powdered mixture of ferroboreon (FeB), ferrotitanium (FeTi) and ferrowolfram (FeW) was used as the coating material. Ferroalloys were used as alloying powder due to their price and low melting temperature. Rectangular plates of ferritic stainless steel (AISI 430, 120 mm long, 50 mm wide and 10 mm thick) were used as substrates in a quenched and tempered condition. The surfaces of the samples were thoroughly cleaned, dried and finally rinsed with acetone. The main chemical compositions of FeB, FeTi, FeW are listed in Table 1. The average size of the ferroalloy particulates was less than 50 µm. In order to obtain a homogeneous distribution of particulates, the combined powders were attrition-milled for 1 h using an agate ball mill with an agate container, and the balls were operated at 300 rpm. The milled mixture with a thickness of 1 mm was fed under the plasma arc (Table 2). Coating was conducted to produce a stable arc by using the PTA process and a tungsten electrode of 3.2 mm in diameter. The arc speed was applied as 0.01 m/min. Table 3 lists the parameters of the coating process. Argon was used as a shielding gas, and the flow rate of the gas was 0.8 l/min.

Table 1. Chemical concentration of the powders used for coating.

	W	Ti	Si	S	Fe	B	C	P
<b>FeTi</b>	-	75	0.5	0.03	Bal.	-	-	0.03
<b>FeB</b>	-	-	1.5	0.04	Bal.	80	7	0.04
<b>FeW</b>	80	-	0.5	-	Bal.	-	-	0.04

The energy given to the surface was controlled as 5 J/cm<sup>2</sup>. Samples were cut from the alloyed samples for microstructural examination and hardness measurements. The samples were prepared for metallographic examination by grinding on SiC wheels followed by polishing and etching with a solution of alcohol and 2% nitric acid. Scanning electron microscopy (SEM) equipped with an energy dispersive X-ray spectrometer (EDS).

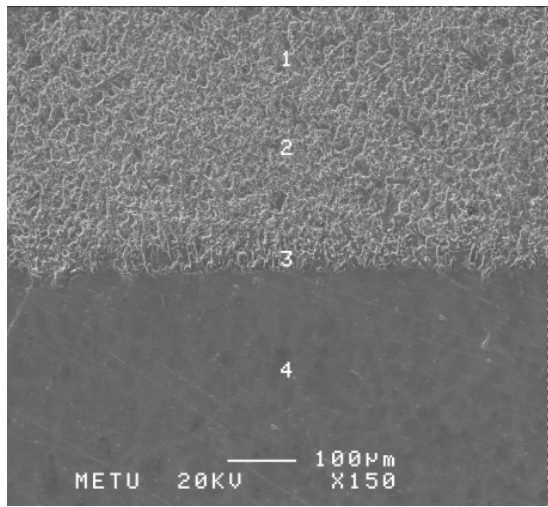
The XRD analysis was obtained by a Rigaku Geigerflex X-ray diffractometry operated at 40 kV and 30 mA using Cu-Kα radiation and X-ray diffraction (XRD) was employed for studying the microstructure and elemental analysis of the coatings. The micro-image analyses with a microprocessor were used to determine the hard phase volume fraction and particle size in the coatings. The average hard phase size and volume fraction were determined by quantitative metallography using a digital image analyser, LEICA Q550. The thermodynamics of the borides were investigated by differential thermal analysis (DTA).

## 3. Results and discussion

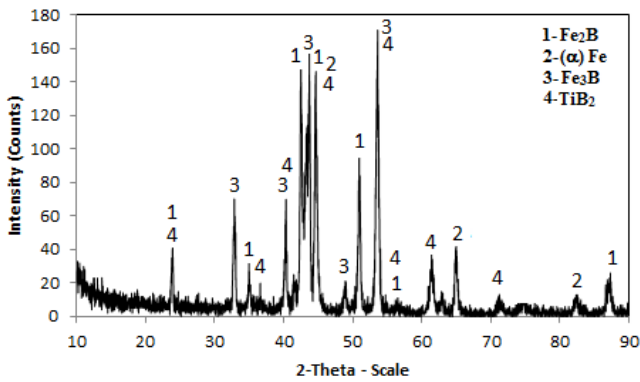
### 3.1. Microstructure of coating

The exothermic dispersion technology [20] was used by applying the PTA to produce a new modified surface in the form of a composite having complex borides (MB<sub>2</sub>-M<sub>2</sub>B) reinforcement particulates. The melting and dilution of the ferroalloy powder mixture to the surface of the substrate resulted in exothermal interaction between the components, and through these reactions, fine hardening particles formed in the solvent phase. Fig. 1 shows the representative microstructure and XRD of the surface coatings of sample S<sub>1,1</sub> (Table 2,3). The Fe based borides are distributed at grain boundaries and Ti based borides uniformly in the matrix of the ferrite phase. On the coated surface of sample S<sub>1,1</sub>, Fe<sub>2</sub>B, FeB and Fe<sub>3</sub>B borides dispersed as 28.5-34.5 vol.% with a particle size in the range of 0.7-3 µm (Table 4). In some studies [20-22] where Ti-B was used, the reinforcement particulates resulted in the formation of TiB<sub>2</sub> with a size of 1-10 µm. The XRD pattern of the coated surface showed that two

types of borides were present: Ti based and Fe based borides (Fig. 1b). The Fe based boride phase mixtures distribution may be ascribed to the interaction between the coating particles and the advancing solid-liquid and liquid-liquid interface. During solidification of molten pool under the arc, the rapid movement of the solid-liquid interface limits the in-situ synthesis of  $Fe_2B$  particles, and brings about a phase mixture of  $Fe_2B$ - $FeB$ - $Fe_3B$  borides in an intergranular form. The decrease of  $FeTi/FeB$  ratio of the cladding coating powders affected the morphology of the microstructure by diffusing the B from boron saturated matrix to grain boundaries during solidification, which then affected the Ti/Fe boride ratio. Fig. 2 shows the SEM micrographs of sample  $S_{1,2}$ , Sample  $S_{1,3}$ , Sample  $S_{1,4}$ .

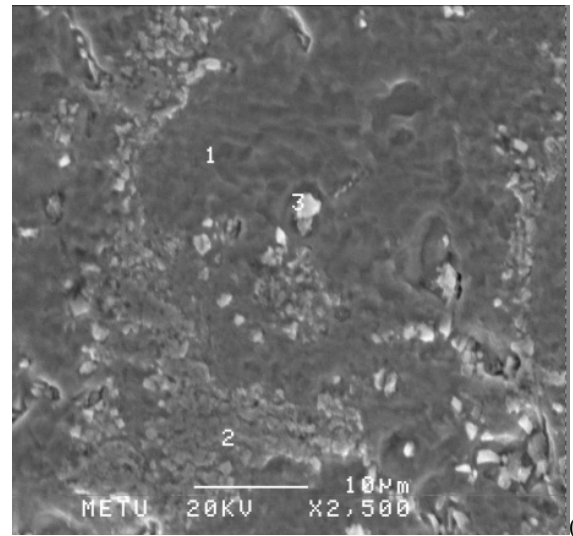


(a)

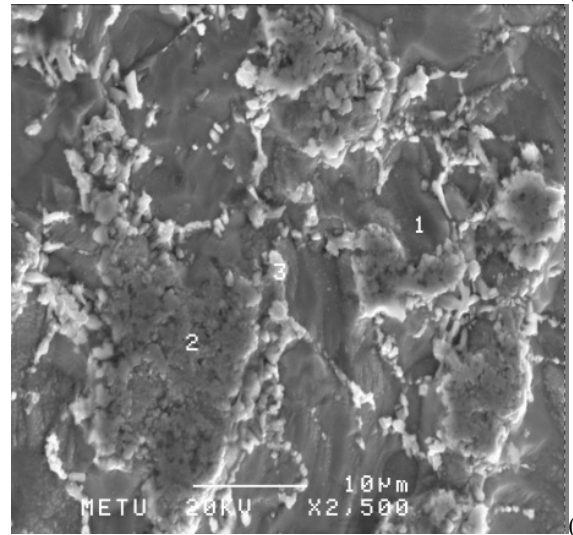


(b)

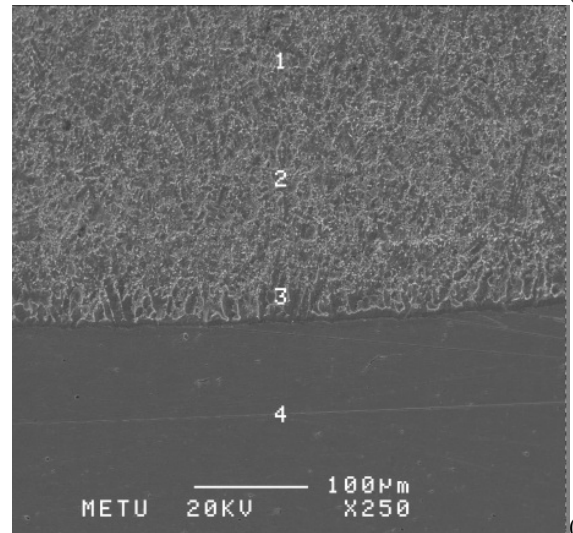
Fig. 1. a) SEM micrographs of sample  $S_{1,1}$ , b) XRD of sample  $S_{1,1}$ .



(a)



(b)



(c)

Fig. 2. a) SEM micrographs of sample  $S_{1,2}$ , b) Sample  $S_{1,3}$ , c) Sample  $S_{1,4}$ .

Fig. 3 shows the change of titanium (wt.%) obtained by EDS analysis from the regions labelled in Fig. 2. Fig. 3a shows the change of Ti (wt.%) at superficial layer. The distribution of Ti at cross-sectional area was plotted by EDS analysis taken from the points 1-4 labelled in Fig. 2. On the other hand, Fig. 3b shows the titanium (wt.%) at matrix and borides, and the EDS analysis taken from the points 1, 2 and 3 in Fig. 2c. The fact that in all cases the amount of Ti is slightly different than expected can be explained by taking into account that during the processing. On the contrary, samples exhibiting secondary borides have a higher proportion of Ti in the  $\alpha$ -phase. Depending on the metallographic investigations, the matrix is ferrite ( $\alpha$ -Fe) having more or less equiaxed  $\text{TiB}_2$  particulates homogeneously distributed in low amount and the second hard phase mixture of Fe borides in irregular shape forming interdendritically in the main. It is seen from the elemental distribution of coated surface that Ti concentration decreased by coming closer from the coated surface to the steel side; on the other hand,  $\text{TiB}_2$  borides homogeneously distributed inside the matrix phase of  $S_{1,2}$  (Fig. 2a,b). The rate determining state for the formation of hard phases is thought to be the reaction of FeTi with FeB during alloying, and the change in kinetic mechanism may be result of the titanium atoms that changes the solubility of the  $\text{TiB}_2$  rather than the boron atoms. Hence, the decrease of the FeTi ratio in cladding powder material decreased the Ti (wt.%) of the borides but increased the vol.% of  $\text{Fe}_2\text{B}$  hard phases (Fig. 2). It is thought that the solidification mechanism is too complex where under the arc, the fine ferroboration particles are melted and merged into streamlets, which arrive at the ferrotitanium particles. The solidified iron nucleus is surrounded by a thick layer of a crystallized liquid whose composition is close to the composition of the  $\text{Fe}+\text{Fe}_2\text{B}$  eutectic melt, according to the EDS results. Upon solidification of this melt, the Fe,  $\text{Fe}_2\text{B}$ , and FeB phases could be found on the corresponding sites of the coating surface (Fig. 2). Increasing in volume, the ferroboration melt covered the solid ferrotitanium particles; at the sites of contact, these particles began to penetrate into the  $\text{FeTi}+\text{Ti}$  (the melting point  $T_{\text{melt}}=1085$  °C) and  $\text{Fe}_2\text{Ti}+\text{Fe}$  ( $T_{\text{melt}}=1290$  °C eutectics). The solidified coated microstructure shown in the Fig. 4 consists of the ferrite grains separated by the eutectic interlayers his shows that boron intensely dissolves in the ferroboration melt, which is a high-boron melt under the plasma arc. After the ferrotitanium particles are melted completely, the ferroboration and ferrotitanium melts form in the coating surface. A layer of titanium diboride continuously forms between the melts, one part of which dissolves as the temperature increases and the other part is carried away by convective liquid flows and is distributed in the form of fine particles in both melts. It seems that the titanium-boron interaction, accompanied by the formation of a contact  $\text{Ti}+\text{TiB}$  liquid, has no time to occur, since when the melting point of this eutectic (1540 °C) is reached in the arc pool, a large amount of liquid phase has already formed in the front on the basis of the other eutectic, which determines the character of the interaction between titanium and boron via this liquid phase. At the moment of

crystallization, quite a homogeneous melt forms in the coating surface, which solidifies to form equilibrium  $\text{TiB}_2$  particles against the background of the  $\text{TiB}_2+\text{Fe}$  eutectic melt (Fig. 4). Thus, three types of titanium boride phases were identified in the final product: primary particles, equilibrium particles from the melt according to the state diagram, and eutectic particles (Fig. 2). In some studies based on Fe-Ti-B systems,  $(\text{Ti,Fe})\text{B}_2$  and  $\text{TiB}_2$  phases were detected in the microstructure [20-23]; however, we observed basically a  $\text{Fe}_2\text{B}$  phase in the grain boundaries. As can be seen in Fig.1, in which XRD traces of  $S_{1,1}$  are shown, secondary borides along with the ( $\alpha$ )-phase are exhibited.

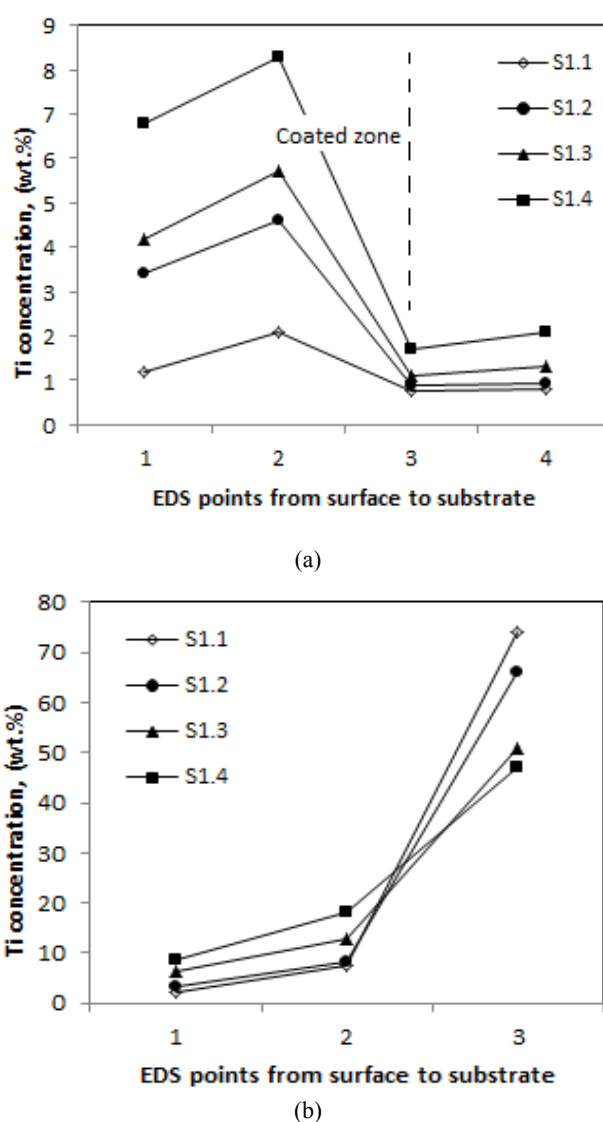


Fig. 3. a) The change of Ti (wt.%) at superficial layer of samples  $S_{1,1}$ ,  $S_{1,2}$ ,  $S_{1,3}$ ,  $S_{1,4}$ , b) The change of Ti (wt.%) at matrix and borides (1:matrix, 2: $\text{Fe}_2\text{B}$ , 3: $\text{TiB}_2$ ).

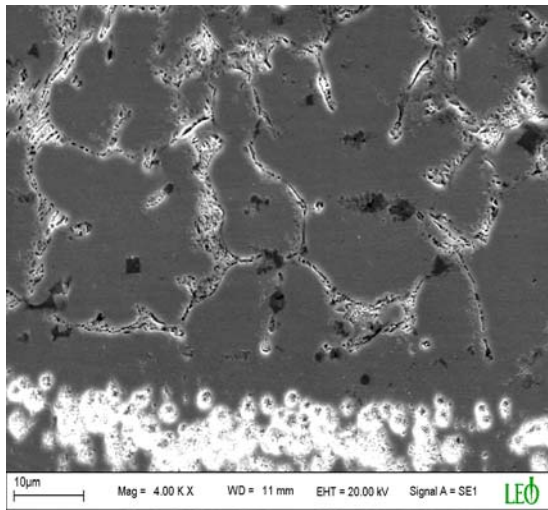
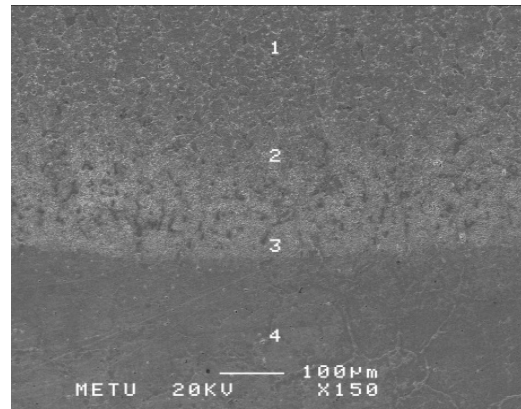


Fig. 4. SEM micrograph of sample  $S_{1.1}$ .

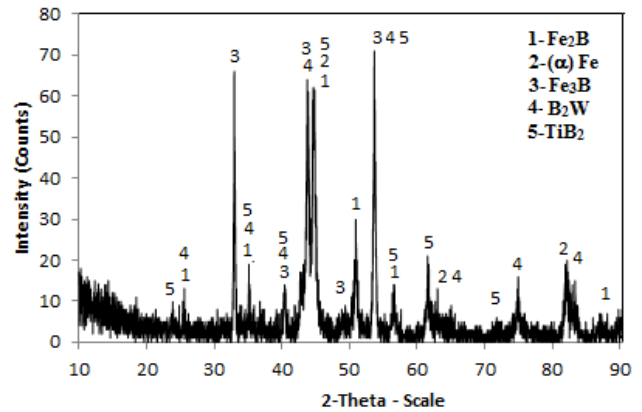
The fracture toughness of  $Fe_2B$  and  $FeB$  borides are lower than  $TiB_2$ , and not sufficient for wear applications. For this reason, the chemical composition of coating material must be adjusted appropriately to decrease Fe based borides and increase  $TiB_2$  borides [9]. It is known that the presence of W activates the formation of  $TiB_2$  as complex  $(TiWB)_2$  boride [9]. Hence, Ferrowolfram ( $FeW$ ) was added to the cladding material, and the samples coated by 10 wt.%  $FeW$  were called as  $S_2$  group (Table 2). The micrographs of the coated surfaces of the samples  $S_{2.1}$ - $S_{2.2}$ - $S_{2.3}$  were shown in Fig. 5. The XRD pattern of the surface composite coatings is shown in Fig. 5b for sample  $S_{2.1}$ , which indicates that the phases present in the coating are mainly rectangular  $TiB_2$ ,  $\alpha$ -Fe and  $WB_2$ . The intermetallic compounds form dendritically during the late stages of solidification. It clearly confirms that  $TiB_2$  particulates can be synthesized by a direct reaction between  $FeTi$  and  $FeB$  in the presence of 10 wt.%  $FeW$ . Depending on the EDS analysis, it was seen that W was seen at matrix as 0.2 wt.% and, rather it is found as dissolved in hard boride particulates as 0.6-0.7 wt.% (Fig. 6).

Table 2. Portions of the powders used for coating (wt.%).

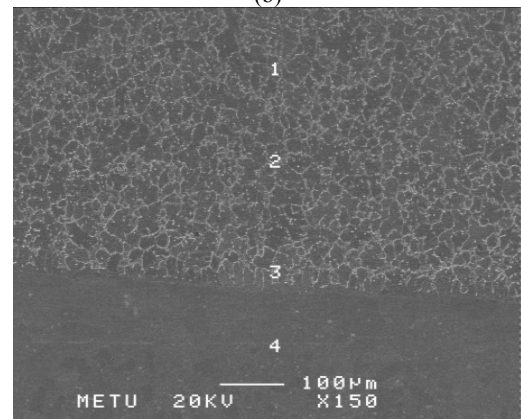
Sample Number	FeTi %	FeW %	FeB %
S1.1	90	--	10
S1.2	80	--	20
S1.3	70	--	30
S1.4	60	--	40
S2.1	80	10	10
S2.2	70	10	20
S2.3	60	10	30
S3.1	70	20	10
S3.2	60	20	20
S3.3	10	10	80



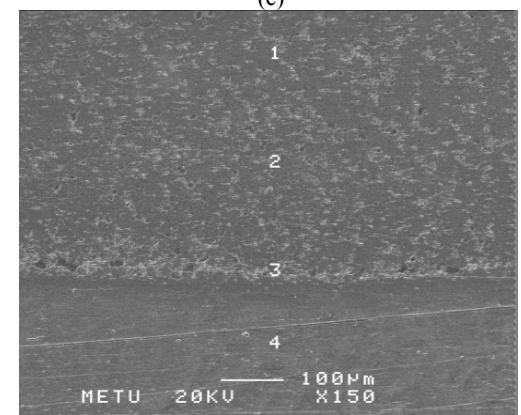
(a)



(b)



(c)



(d)

Fig. 5. a) SEM micrograph of sample  $S_{2.1}$ , b) XRD results of sample  $S_{2.1}$ , c) SEM micrograph of sample  $S_{2.2}$ , d) SEM micrograph of sample  $S_{2.3}$ .

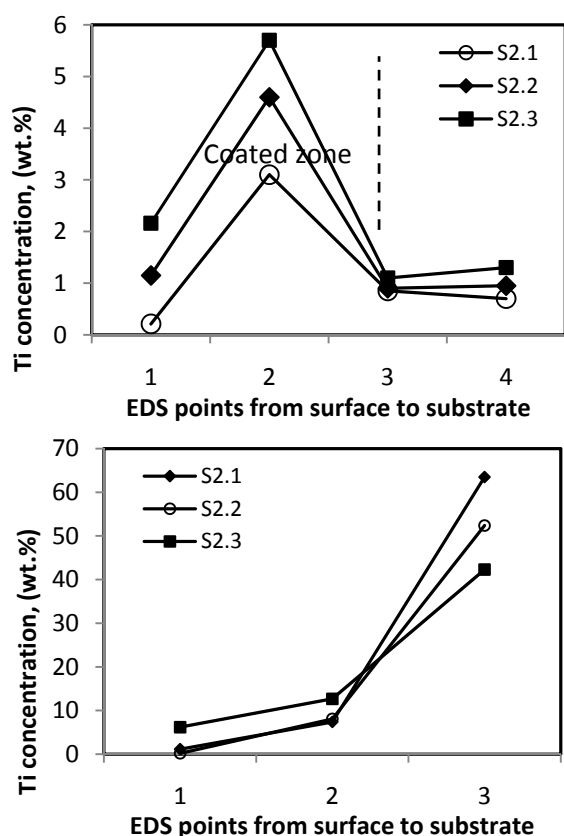


Fig. 6. a) The change of Ti wt. % at coated surface of sample  $S_{2.1}$ ,  $S_{2.2}$ , and  $S_{2.3}$ , b) Ti wt.% at matrix and borides (1:matrix, 2: $Fe_2B$ , 3: $TiB_2$ ).

A small change in the Ti ratio changes the chemical composition of the liquid solution, causing a shift in the structure from  $TiB_2$ -Fe binary phase equilibrium to  $TiB_2$ -Fe- $Fe_2B$ . It is seen in Fig. 6 that the chemical composition of Ti in the  $TiB_2$  phase decreased from 68 to 40 wt.% by decreasing the ratio of FeTi powders from 80 to 70 wt.% (Table 2). Using the above considered technique, one can determine the sequence of the processes in the coating of the second group of samples from the results of structural studies. The final product is a result of the solidification of the melt. As in the first case, the appearance of the liquid

phase in the coating is due to the contact melting of the charge components and substrate. When considering the structure formation in the coating, we assumed that the liquid phase forms on the sites of particle contact as a result of contact melting, according to the diffusion-free mechanism, which implies that the following two factors are sufficient for the liquid phase to appear in the coating: the contact between the particles and the corresponding temperature [8]. The EDS microanalysis showed that there is iron in the titanium boride particles with a changed microstructure. These points to the solid phase character of the initial stage of the titanium boron interaction (Fig. 5c-d). The first portions of the liquid phase appear in the system when the temperature corresponds to the FeTi low-temperature eutectic melt. Possibly, when the temperature corresponding to the second  $Fe_2Ti+Fe$  eutectic melt is reached, the liquid phase of another composition forms at the contact sites. After the appearance of the liquid phase in the system, the ferrobiron-ferrotitanium interaction occurs via the contact melt in which iron, boron, titanium and wolfram dissolve as the temperature increases. When the liquid phase forms, probably ferrobiron, ferrotitanium and ferrowolfram particles partially disperse in the molten pool. The fine initial and dispersed FeB particles dissolve rapidly in the ferrotitanium melt, saturating it with wolfram and boron. The coarse ferrobiron particles are gathered by the contact melt in a conglomerate. At the interface between this conglomerate and the melt, the  $TiB_2$  layers forms. Ferrotitanium dissolves completely in the intermediate melt, which contacts extensively with the rest of the ferrobiron particles. In Fig. 5d the ferrobiron regions bordering the melt are light-coloured. As the EDS analysis shows, these are the regions of almost pure iron which were formed as a result of the intense diffusion of boron into an "intermediate" melt. In the ferrobiron particles, the interfaces between the grains, where the diffusion flows primarily occur, are depleted of boron too (Fig. 6). After the rest of the ferrobiron has melted completely through the intermediate melt, near the region, a concentration-inhomogeneous melt forms; this melt crystallizes to yield titanium borides and several types of structure:  $WB_2$ , and  $Fe_3B$  (Fig. 5b).

Table 3. PTA operating parameters.

Current (A)	Plasma Gas Flow (l/min.)	Shielding Gas Flow (l/min.)	Traverse Speed (m/min.)	Nozzle Diameter (mm)	Powder feeding ( $gs^{-1}$ )	Coating size ( $\mu m$ )			
						dc	hc	tc	wc
130	0.8	20	0.01	3.2	1.5	260	320	570	400

dc: maximum depth (above the original substrate surface, hc: max. height above the original substrate, tc: maximum total coating thickness (dc+hc), wc: maximum width.

In order to make a thermodynamic approach based on the general trends, data published in the literature [24-26] must be considered. As it concerns the Fe-Ti-B system, a quasi-binary section can be found along the line  $TiB_2$ -(Fe, 2 at.% Ti), characterised by a simple eutectic. Below this amount of Ti,  $Fe_3B$  coexists with  $TiB_2$ . In the W-Ti-B system, the presence of a  $W_2B$  is due to the dissolution of

$Fe_3B$  in FeCr at the eutectic temperature. In addition, it must be pointed out that  $Fe_3B$  is the minimum Ti-containing phase which can coexist with  $TiB_2$  in the absence of the  $W_2B$ . It was seen that the addition of the FeW to the coating powders increased the hard phase ratio at coated surface structure (Table 4). Due to the fact that a higher minimum amount of Fe is required, increasing

proportions of Ti should be related to the highest heat of reaction of  $W_2B$  associated with W-rich Fe-W-Ti alloys. In the studied composition range, the equilibrium state expected is the maximum amount of  $TiB_2$ . Regarding the

third group, the concentration of the FeW in cladding powders of second group increased from 10 wt.% to 20 wt.%.

Table 4. The hard phase ratio, surface hardness and micro hardness of hard phases and matrix of coated surfaces.

Sample	$TiB_2$ (HV)	$Fe_2B$ (HV)	Hard phase ratio (Vol. %)	Matrix (HV)	Surface hardness (HRc)
S <sub>1,1</sub>		1500-1700	28	600-680	42.87
S <sub>1,2</sub>		1550-1700	31	670-700	46.22
S <sub>1,3</sub>		1600-1700	32	800-900	47.82
S <sub>1,4</sub>		1600-1700	34	800-900	48.65
S <sub>2,1</sub>		1600-1700	33	800-1000	49.93
S <sub>2,2</sub>	2300-2400	1300-1450	34	800-1000	51.15
S <sub>2,3</sub>	2300-2400	1300-1450	35	800-1000	52.25
S <sub>3,1</sub>	2300-2400	1300-1450	34	800-1000	51.75
S <sub>3,2</sub>	2700-3000	1500-1700	39	800-1000	53.70
S <sub>3,3</sub>	3100-3300	1500-1700	43	900-1100	55.26

The SEM micrographs of the coated surface of the S<sub>3</sub> group samples that were coated with a cladding powder mixture of (FeTi-FeW-FeB) are given in Fig. 7. As seen from the microstructure and EDS analysis (Fig. 7), W was dissolved in the matrix. The existing phase of the coated surface of the third group is mainly  $TiB_2$ ,  $WB_2$  and  $\alpha$ -Fe (Fig. 7d). The intermetallic compound of  $Fe_2B$  was not observed for the samples coated by the FeW-FeB-FeTi powder mixture. The  $TiB_2$  phase was formed homogenously and in a rectangular form. The borides with a 900-1100 °C melting temperature and appropriate

wetting character were not formed. The diborides of IV-VI group metals dissolve at temperatures of 2000-3000 °C, and the atomic size difference between the elements decreases the dissolution temperatures [27-28]. For this reason, it is thought that W activated the formation of  $TiB_2$  at 2000 °C. The EDS analysis shows that the hard particulates are  $(Ti,Fe)B_2$  when the concentration of cladding powders have about 70 wt.% FeTi (Table 2). But the decrease of FeTi powder concentration in cladding powders from 70 to 60 wt.% changed the type of boride from  $(Ti,Fe)B_2$  to  $(Fe,Ti)_2B$  (Fig. 7d).

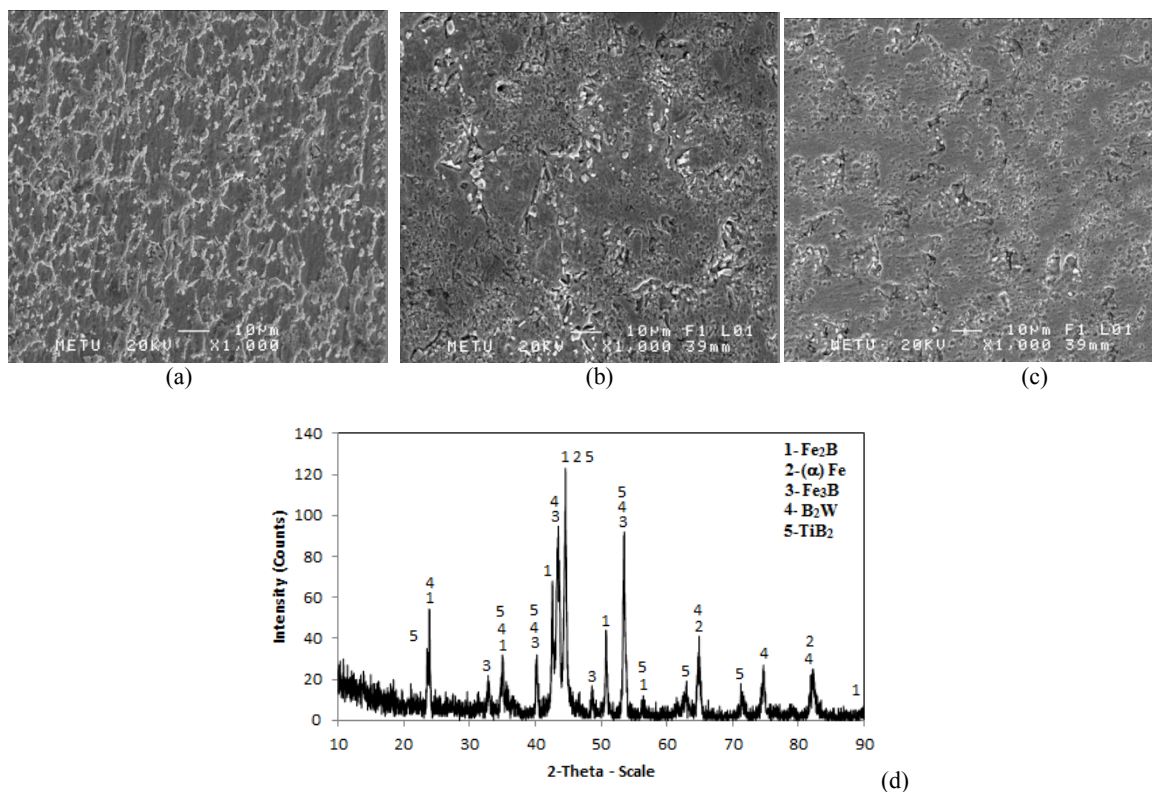


Fig. 7. SEM micrograph of a) Sample S<sub>3,1</sub>, b) Sample S<sub>3,2</sub>, c) Sample S<sub>3,3</sub>, d) XRD of sample S<sub>3,3</sub>.

The chemical analysis taken from the borides shows that Ti concentration in hard reinforcement phases are 65 wt.% for sample  $S_{3,1}$ , 19.23 wt.% for sample  $S_{3,2}$ , and 3.61 wt.% for sample  $S_{3,3}$ , which show that the B wt.% of reinforcements substantially dependent on the FeTi/FeTi ratio (Fig. 8). The  $TiB_2$  phase can be present with FeB,  $Fe_2B$ ,  $\alpha$  or  $\gamma$ -Fe,  $FeTi_2$  and FeTi phases [28]. The samples coated by FeB+FeTi+FeW powders have shown that W decreased the hard phase ratio; on the other hand,  $TiB_2$  hard phases were seen in these samples. Three types of borides,  $(Ti,W)B_2$ ,  $(Ti,W)B_2$  and  $(W,Ti)_2B_5$ , can form in the Ti-W-B system [23]. However,  $(Ti,W)B_2$  phases were not observed for the samples  $S_{3,1}$ - $S_{3,2}$ - $S_{3,3}$  in this work. For formation of the maximum  $TiB_2$  and minimum  $FeB_2$  phases the best coating powder ratio (FeW:FeTi:FeB) was seen in the composition of  $S_{3,2}$ . From XRD results it was seen that the increase of the W in the powder decreased the  $Fe_3B/TiB_2$  ratio by up to 0.65. In addition, the increase of the FeW ratio from 10% to 20% decreased the  $W_2B/TiB_2$  ratio from 1 to 0.7 (Fig. 8).

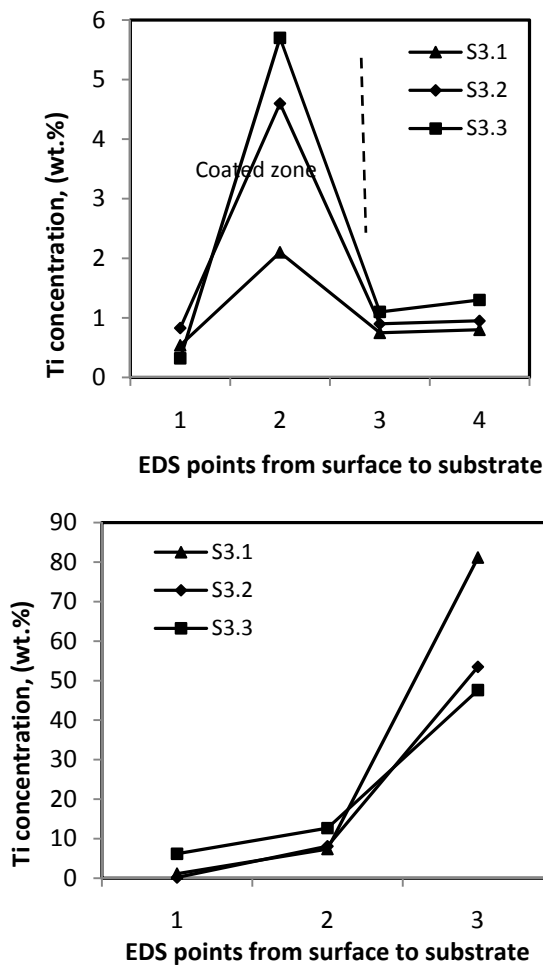


Fig. 8. a) The change of Ti wt.% at coated surface of sample  $S_{3,1}$ ,  $S_{3,2}$ , and  $S_{3,3}$ , b) Ti wt.% at matrix and borides (1:matrix, 2: $Fe_2B$ , 3: $TiB_2$ ).

### 3.2. DTA of coating

DTA of coating surfaces were shown in Table 5. DTA analysis of sample  $S_1$  group shows that  $\gamma$ -Fe dissolves to  $\alpha$ -Fe phase at 760-1050 °C temperatures intervals. By reaching 1100 °C temperature,  $TiB_2$  is in equilibrium with FeB,  $Fe_2B$ ,  $\alpha$ -Fe,  $Fe_2Ti$  phases [20]. It was observed that  $TiB_2$ -Fe binary system is in equilibrium with  $FeB_2$  at 1167 °C. Furthermore, system has solid  $\alpha$ -Fe instead of liquid  $\alpha$ -Fe phase at 1167 and 1268 °C. During 1200-1300 °C temperature interval the  $Fe_2B$  boride dissolved, and  $TiB_2$  is in eutectic equilibrium with liquid Fe over 1268 °C temperature. In some studies at eutectic point and 1340 °C temperature, Fe-TiB<sub>2</sub> pseudo-binary equilibrium was seen [17,19]. The increase of FeB powder rate, from 10 (wt.%) to 20, of coating material increased the dissolution temperature of  $\gamma$ -Fe, but the addition of FeW ferro-alloy powder did not change the dissolution temperature of  $\gamma$ -Fe in high rates, but increased the  $\gamma$ -Fe to  $\alpha$ -Fe dissolution temperatures from 900 to 1100 °C temperatures. On the other hand, FeW powder addition to coating material did not affect the dissolution temperatures of  $Fe_2B$  boride phase, on the other hand decreased the enthalpy of this reaction from 370 J/g to 45 J/g.

For  $S_3$  group the dissolution temperature of  $\gamma$ -Fe to  $\alpha$ -Fe reaction is near to  $S_2$  group (Table 5). However, the enthalpy of this reaction decreased and the dissolution of  $Fe_2B$  phase did not seen. In some studies; Fe was accepted as a binder phase for  $TiB_2$ , but in this study the formation of  $Fe_2B$  is unavoidable, and a Fe solid solution is in equilibrium with Ti. The first liquid phase appears at 1270 °C coming from the Fe- $FeB_2$  eutectic.  $TiB_2$  is compatible with Ti bearing ferrite only below 928 °C.  $TiB_2$ - $\alpha$  Fe contains  $FeB_2$  below 1167 °C, and between 928 and 1148 °C solid  $\gamma$  or  $\alpha$ -Fe are absent.

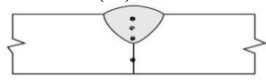
Table 5. DTA analysis of samples giving dissolution temperatures and enthalpy changes.

Sample	$\gamma$ Fe $\rightarrow$ $\alpha$ Fe		$Fe_2B \rightarrow$ Liquid	
	T, °C	$\Delta H$ , J/g	T, °C	$\Delta H$ , J/g
S1.1	964	-405	1281	-4,3
S1.2	975	-465	1272	-5,6
S1.3	987	-1000	1220	-85
S1.4	1097	-221	1215	-200
S2.1	1073	-7155	-	-
S2.2	1084	-7280	-	-
S2.3	1096	-7450	-	-
S3.1	928	-5130	-	-
S3.2	1148	-9960	-	-
S3.3	1113	-10160	-	-

### 3.3. Hardness of the coating

The hardness of the coated surface reinforced by TiB<sub>2</sub>, WB<sub>2</sub> and Fe<sub>2</sub>B borides was determined along the depth from the irradiated surface; all the data was an average of three measurements. The variations of the hardness across the transverse cross-section of the coating are presented in

Table 6. Macrohardness via layer depth of the PTA processed coating.

Sample No	S1.1	S1.2	S1.3	S1.4	S2.1	S2.2	S2.3	S3.1	S3.2	S3.3
Rockwel (A)	57	59.7	61.5	58.7	59.3	52.6	60.1	59.7	59.1	58,3
	56.3	58.8	55	53.4	57	59.7	57.6	58	63	60.2
	52.6	52.7	54.4	52.6	57.9	57	59.1	53.1	57.7	59.4
	54.2	55.7	54	53.4	53.9	54.4	54.1	56	54.2	55.3

The hardness of the coating progressively decreased from the surface to the substrate. It was noted that there is no sudden transition from the coating to the substrate in terms of the hardness, which indicates an absence of a sharp demarcation in materials' properties across the interface. Furthermore, the average hardness of the coating gradually increased with an increase in the content of TiB<sub>2</sub> and Fe<sub>2</sub>B, which was due in part to the formation of more particles during PTA processing. The highest hardness value was obtained from the coated sample having a 39 vol.% hard phase ratio. The matrix hardness also changed depending on the coating powder ratio. The reported hardness value of TiB<sub>2</sub> varies from 2900 HV [29] to 3400 HV [30]. The measured hardness value of TiB<sub>2</sub> falls within the reported range. The measured hardness of Fe<sub>2</sub>B matches the literature value [31, 32].

### 4. Conclusions

1. A new in-situ method has been developed to produce a metal matrix composite with TiB<sub>2</sub>, Fe<sub>2</sub>B and W<sub>2</sub>B reinforcing particles by alloy surface composite coating on AISI 430 stainless steel by PTA. Complex TiB<sub>2</sub> particles were synthesized from FeB-FeTi-FeW powder mixture, and a coated surface having homogeneously distributed borides in the size of 1-5 μm were obtained.

2. The FeTi/FeB ratio in cladding powders increased up to 3/2, and the Fe<sub>3</sub>B/TiB<sub>2</sub> boride phase ratio decreased substantially to 4. The reinforcement phase is formed at the 3-5 μm size, ≈34.5(vol.%).

3. Addition of ferroboreon to the mixtures leads to the (TiW)B<sub>2</sub> phase which are intermetallic compounds, mainly spherical. The hard phases in the coating were mainly ≈35(vol.%) TiB<sub>2</sub>, and Fe<sub>3</sub>B intermetallic compounds.

4. Completely (TiW)B<sub>2</sub> hardened microstructure are obtained with an alloying powder having FeTi-FeW-FeB mixture for sample S<sub>3.2</sub>. The chemical composition and (vol.%) of borides change as the ratio of the powders used in alloying mixture. Ti and W elements were dissolved in the matrix of the sample S<sub>3</sub> group samples. The highest TiB<sub>2</sub> concentration was seen for the sample S<sub>3.3</sub> having ≈43(vol.%). The usage of FeW:FeTi:FeB ratio as 20:60:20

prevented the formation of unwanted Fe<sub>3</sub>B phase, and the Fe<sub>3</sub>B was seen as (Fe<sub>3</sub>B/TiB<sub>2</sub>=0.6).

5. The formation of Fe<sub>2</sub>B boride consumes a substantial fraction of the ductile Fe phase such that Fe<sub>2</sub>B is believed that it makes brittle the coated surface seriously. The usage of FeW hold up the formation of that phase, which was a major goal for developing and increasing vol.% of tough TiB<sub>2</sub> phase, and where DTA results of this study are is proportional with XRD results.

6. The usage of titanium, tungsten, boron elements from ferro-alloys brings an extremely cheap production cost.

### Acknowledgements

The authors gratefully acknowledge the assistance of the Committee of Scientific Research/FUBAP for its support of this research (Grant No.1641). The authors would like to also gratefully acknowledge the use of the laboratory facilities at Firat University, Turkey.

### References

- [1] Y. F. Liu, Z. Y. Xia, J. M. Han, G. L. Zhang, S. Z. Yang, Surf. & Coat. Technol. **201**, 863 (2006).
- [2] R. L. Deuis, J. M. Yellup, C. Subramanian, Compos. Sci. Technol. **58**, 299 (1998).
- [3] L. W. Tsay, Z. W. Lin, R. K. Shiue, C. Chen, Mater. Sci. & Eng. A. **290**, 46 (2000).
- [4] X. Tian, P. K. Chu, Scripta Mater. **43**, 417 (2000).
- [5] K. Holmberg, A. Matthews, H. Ronkainen, Tribology Int. **31**, 107 (1998).
- [6] Y. G. Fu, J. Wei, A. W. Batchelor, J. Mater. Proces. Tech. **99**, 231 (2000).
- [7] M. Zapponi, A. Quiroga, T. Pe'rez, Surf. & Coat. Tech. **122**, 18 (1999).
- [8] R. A. Hadfield, Metallurgy and its influence on modern progress, Chapman and Hall Ltd., London, 1925, pp. 91-101.
- [9] P. J. Modenesi, E. R. Apolinario, I. M. Pereira, J. Mater. Process. Technol. **99**, 260 (2000).

- [10] Z. M. Zeng, T. Zhang, B. Y. Tang, X. B. Tian, P. K. Chu, *Surf. & Coat. Tech.* **120-121**, 659 (1999).
- [11] R. W. Cahn, *The encyclopedia of ignorance*, Pergamon Press, New York, 1977, pp. 140.
- [12] V. Raghavan, K. S. Raghavan, S. A. Sastri, M. J. Marcinkowsky, *Acta Metall.* **17**(10), 1299 (1969).
- [13] J. Stringer, *Surf. & Coat. Tech.* **108-109**, 1 (1998).
- [14] C. N. Panagopoulos, A. E. Markaki, P. E. Agathocleous, *Mater. Sci. & Eng. A.* **241**, 226 (1998).
- [15] R. W. Smith, A. De Monte, W. B. F. Mackay, J. *Mater. Process. Technol.* **153-154**, 589 (2004).
- [16] H. Pastor, *Boron and Refractory Borides*, Springer-Verlag, Berlin, 1977, pp. 457.
- [17] F. De Mestraland, F. Thenevot, *Mater. Sci.* **26**, 5547(1991).
- [18] L. Ottavi, C. Saint-Jours, N. Valignant, C. Allibert, *Z. Metallkd.* **83**, 80 (1993).
- [19] L. S. Sigland, Th. Jungling, *J. Hard Mater.* **3**, 39 (1992).
- [20] I. Goldfarb, M. Bamberge, *Scripta Mater.* **34**(7), 1051 (1996).
- [21] Z. Zeng, J. Zhang, *Surf. & Coat. Tech.* **202**(12), 2725 (2008).
- [22] K. Satyaprasad, Y. R. Mahajan, V. V. Bhanuprasad, *Scripta Metall. Mater.* **26**(5), 711 (1992).
- [23] G. Petzow, R. Telle, R. Danzer, *Mater. Charact.* **26**(4), 289 (1991).
- [24] V. M. Zalkin, *Nature of eutectic melts and the effect of contact melting*, Metallurgiya, Moscow, 1987, pp. 150.
- [25] A. K. Shuringand, B. E. Panarin, *Russian Metall.* **5**, 192 (1974).
- [26] R. Luck, H. Wang, B. Predel, *Z. Metallkd*, Experimental, Thermody-namic Calculation, in German, **82**, 805 (1991).
- [27] K. Nishiyama, S. Umakawa, *Achievements in Composites in Japan and the United States*, Kobayashi, A.(Ed.). *Proc. 5th Japan-US Conference on Composite Materials Tokyo, 1990*, pp. 371-378.
- [28] T. J. Jüngling, L. SSigl, R. Oberacker, F. Thümmeler, K. A. Schwetz, *Int. J. Refrac. Metals and Hard Mater.* **12**(2), 71 (1993-1994).
- [29] G. Hilz, H. Holleck, *Mater. Sci. & Eng. A.* **139**, 268 (1991).
- [30] B. S. Terry, A. S. Chinyamakobvu, *Mater. Sci. Technol.* **8**, 491 (1992).
- [31] C. C. Degnan, P. H. Shipway, *Metal. Mater. Trans. A.* **33**, 2973 (2002).
- [32] E. Pagounis, M. Talvitie, V. K. Lindroos, *Powder Metal.* **40**, 55 (1997).

\*Corrospounding author: tteker@adiyaman.edu.tr